Three-dimensional modeling of fugitive dust dispersion in idealized openpit mines

by T. Bhowmick, K.V. Raj and S. Bandopadhyay

Abstract ■ The control of fugitive dust in high-latitude openpit mines is challenging due to unique atmospheric phenomena resulting in complicated flow regimes as well as atmospheric inversion due to the lack of adequate insolation during prolonged winter seasons. In this study, two idealized (one conical and one trapezoidal) three-dimensional openpit mine geometries were simulated for different seasonal conditions using a computational-fluid-dynamics package from Software Cradle. The airflow was solved by Reynolds-averaged Navier-Stokes equations using the standard kappa-epsilon turbulence model. The concept of particle tracking was used to predict the flow patterns of dust particles.

For various climatic conditions and two different pit geometries, fugitive dust particles varying in size, from $PM_{0.1}$ to PM_{10}, and concentration were generated at various locations and dispersed by the airflows inside the openpit mine. The amount and location of dust particles inside the pit were reported at various time intervals. In the summer season, airborne dust particles were quickly transported outside the openpit domain. In the winter season, however, the development of atmospheric inversion significantly affected the amount of dust retention inside the openpit domain.

Mining Engineering, 2015, Vol. 67, No. 10, pp. 45-52.
Official publication of the Society for Mining, Metallurgy & Exploration Inc.

Introduction

The computational-fluid-dynamics (CFD) modeling of openpit mines is challenging. In a recent paper (2015), we presented different constraints and challenges in developing a three-dimensional CFD model. In order to obtain realistic results from a simulation, however, appropriate values of various inputs are required. The simulation results of a three-dimensional nonhydrostatic model by Shi et al. (2000) showed that both the mechanical and thermal forces are important mechanisms, controlling the development of the atmosphere inside an openpit mine. Alvarez et al. (2007) used a CFD model for predicting dust dispersions in a medium-sized limestone quarry, and presented several iso-surfaces of varying dust concentrations using ANSYS CFX. A similar study by Torno et al. (2010) introduced a more sophisticated parameterization of the dust sources. Flores et al. (2014) used an OpenFOAM CFD simulation package to simulate and predict pollutant dispersion in an idealized and an actual openpit mine in Chile with an intense insolation condition. The model was simulated for three different conditions: (1) air-advection (10 m/s, or 33 ft/sec)-driven mechanical turbulence, (2) surface-heat-flux (240 W/m^2, or 76 Btu/ft^2-h)-driven thermal buoyancy and (3) both air-advection- and surface-heat-flux-driven conditions. The results of the simulations showed that the buoyant currents contribute to the removal of a large percentage of the dust particles. The buoyant currents modify the purely mechanical-turbulence-induced flow pattern and reduce the particle residence time, commonly observed in a purely mechanical turbulent flow (nonbuoyant case).

In this study, we used four-component net-radiation and temperature sensors to obtain the micrometeorological data for the input boundary conditions. Wind-velocity profiles were obtained from a weather station near the selected openpit mine. The obtained data indicated different climatic conditions in various seasons. Furthermore, due to the different climatic conditions, the behavior of the airflow changes completely from one season to another.

In this paper, the changing climatic conditions in the selected openpit mine were obtained for various seasons. Two

T. Bhowmick, K.V. Raj and S. Bandopadhyay, members SME, are M.S. student, Ph.D. student and professor, respectively, at the University of Alaska Fairbanks, Fairbanks, AK. Paper number TP-14-055. Original manuscript submitted November 2014. Revised manuscript accepted for publication March 2015. Discussion of this peer-reviewed and approved paper is invited and must be submitted to SME Publications by Jan. 31, 2016.

Resumen ■ El control de polvo fugitivo en minas a tajo abierto en latitudes elevadas es desafiante debido a fenómenos atmosféricos propios de esas regiones que resultan en regímenes de flujo complicados, así como inversiones atmosféricas por causa de falta de una adecuada insolación en temporadas invernales prolongadas. En este estudio se realizó una simulación idealizada (una cónica y la otra trapezoidal) de geometrías tridimensionales de minas a tajo abierto para diferentes condiciones estacionales usando un paquete de mecánica de fluidos computacional (CFD por sus siglas en inglés) de Software Cradle. El flujo de aire fue resuelto por ecuaciones de Navier-Stokes con el promedio de Reynolds usando el modelo estándar de turbulencia kappa-epsilon. Se usó el concepto de rastreo de partículas con el fin de predecir los patrones de flujo de partículas de polvo.

Con el fin de ver los efectos en diferentes condiciones climáticas y en dos geometrías de tajos diferentes se generaron partículas de polvo fugitivo de diferente tamaño, de $PM_{0.1}$ a PM_{10}, y en diferentes concentraciones en distintos lugares y se dispersaron mediante flujos de aire al interior de la mina abierta. Se reportó la cantidad y ubicación de partículas de polvo dentro de la mina en diferentes intervalos de tiempo. En la temporada de verano, las partículas de polvo en el aire fueron rápidamente transportadas fuera del área del tajo abierto de la mina. Sin embargo, en el invierno, la inversión atmosférica afecto de manera significativa la cantidad de retención de polvo dentro del área del tajo abierto.

Figure 1

SW and LW radiation plot inside the openpit on Dec. 4, 2013.

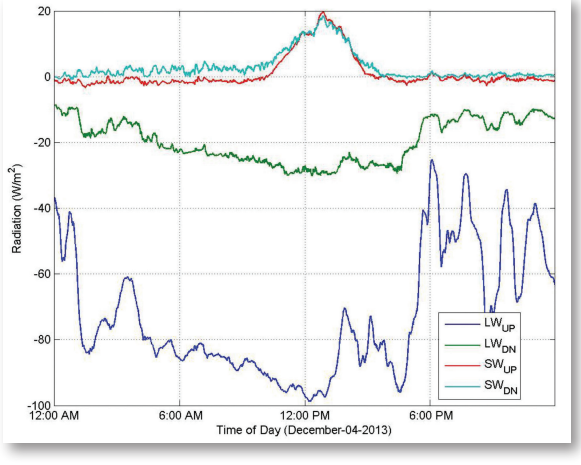

idealized (one conical and one trapezoidal) three-dimensional openpit mine geometries were developed for CFD modeling. Different boundary conditions due to the various seasons were defined in the models. Dust particles were generated at various locations of the domain to represent the sources of fugitive dust particles in an openpit mine.

Climatic conditions

The atmospheric boundary layer (ABL) is the part of the troposphere that is directly influenced by the presence of the Earth's surface and responds to the surface forcing in a time scale of about one hour or less (Stull, 1988). Micrometeorological and ABL flows are developed due to the (1) surface energy balance, (2) surface roughness and (3) influences of mesoscale and synoptic-scale flows in the atmosphere. In micrometeorological flow, the surface energy balance and surface roughness play dominant roles due to the shorter special and temporal scales of the micrometeorology. For

Figure 2

RN plots inside the openpit on (a) Dec. 4, 2013 (b) June 27, 2014.

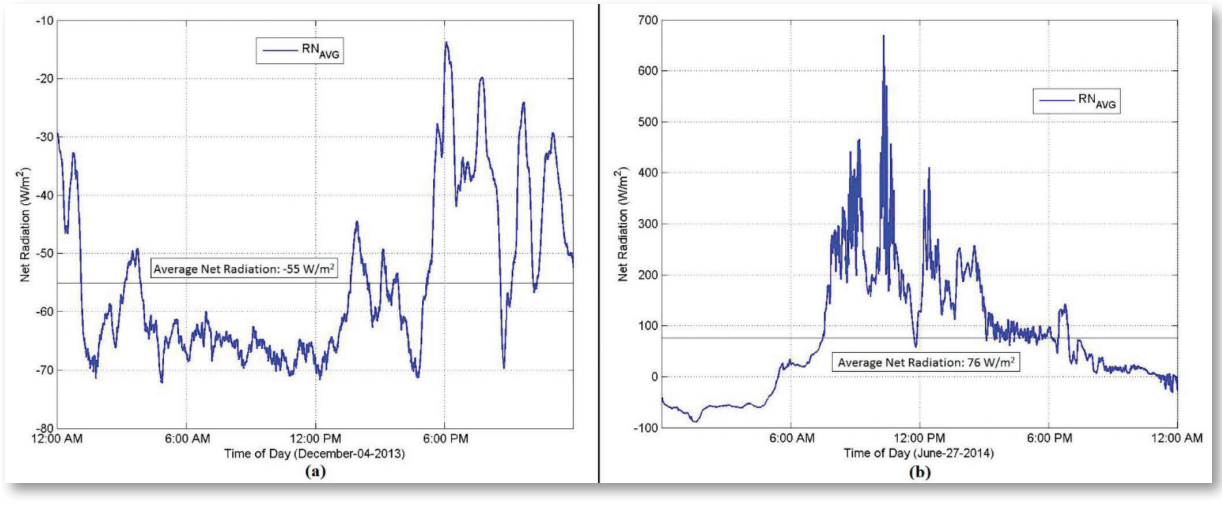

Figure 3

Temperature and wind-speed variations from Dec. 1, 2013, to Jan. 31, 2014. (Source: www.wunderground.com)

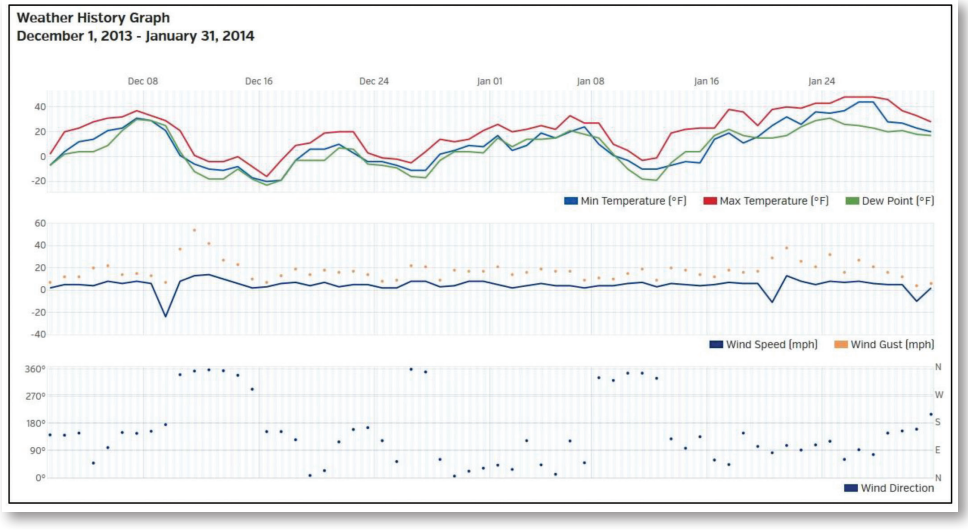

fugitive dust dispersion in an openpit domain, the development of micrometeorological and ABL flows in the domain is rather important, since the dust dispersion is directly influenced by these two types of flow.

The surface energy balance is an energy balance that results from net radiation (RN), ground heat flux (G), sensible heat flux (H) and latent heat flux (LE). The RN component in the energy balance equations shown as Eqs. (1) and (2) results from shortwave (SW) and longwave (LW) radiation, both downwelling (DN) and upwelling (UP):

$$RN - G = H + LE \quad (1)$$

$$RN = SW_{DN} + SW_{UP} + LW_{UP} + LW_{DN} \quad (2)$$

In the selected openpit mine, no water surface is present. Therefore, the LE component in Eq. (1) is ignored due to the absence of any latent heat, and the G component, which is a small fraction of RN, is also ignored for simplification purposes. From Eq. (1), it is clear that the RN from the openpit surface is used entirely as H, which results in temperature variation in airflow inside the openpit mine. Figure 1 presents a plot of SW and LW radiation obtained from the four-component radiometer installed inside the selected openpit mine on Dec. 4, 2013, and Fig. 2a shows the resultant RN from the SW and LW radiation. Figure 2b shows the resultant RN from the SW and LW radiation in summer, on June 27, 2014. A completely different radiation phenomenon is observed between the summer and the winter seasons inside the openpit mine. The RN plots varied between −70 and −14 W/m^2 (−22 and −4.4 Btu/ft^2-h) on the winter day (Fig. 2a) and 700 and −100 W/m^2 (222 and −32 Btu/ft^2-h) on the summer day (Fig. 2b). As the "variable input heat flux" option is unavailable in the SC/Tetra software, from Software Cradle Co. Ltd., the input values of heat flux were averaged based on the intensity of the seasonal condition, and a constant input heat flux was provided in each simulation. The average values of net radiation in Figs. 2a and 2b are −55 and 76 W/m^2 (−17 and 24 Btu/ft^2-h), respectively. Similarly, based on the average values of net radiation in the remaining days of the winter and the summer season, the input heat flux values

Table 1

Input values for the winter and the summer sessions.

Season	Intensity	Wind speed	Initial temperature	Heat flux (W/m^2)
Winter	Moderate winter	4.7 mph = 2.1 m/sec	−10°C	−20
	Extreme winter	4.7 mph = 2.1 m/sec	−10°C	−40
Summer	Fair insolation	5.6 mph = 2.5 m/sec	10°C	60
	Moderate insolation	5.6 mph = 2.5 m/sec	10°C	100
	Extreme insolation	5.6 mph = 2.5 m/sec	10°C	160

Figure 4

Idealized (a) trapezoidal and (b) conical openpit domains.

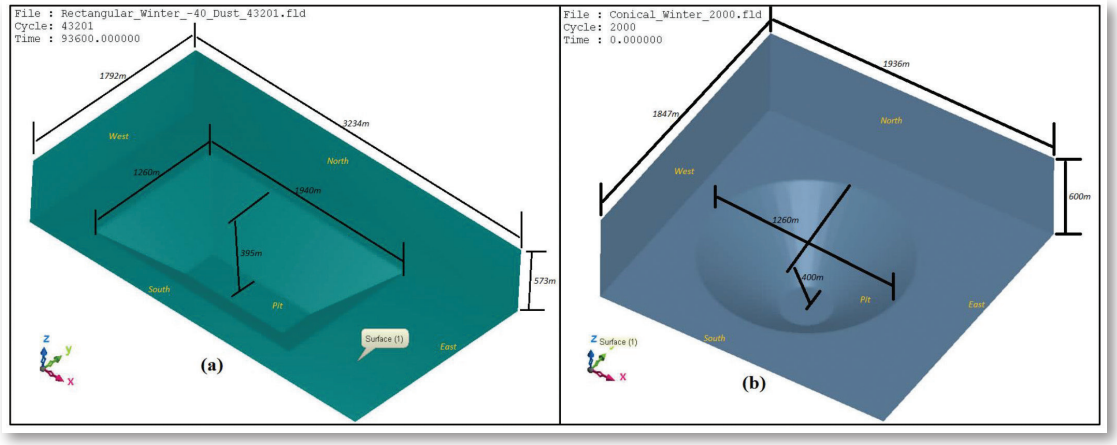

for the moderate and extreme winter and fair, moderate and extreme summer conditions were defined to be −20, −40, 60, 100 and 160 W/m^2 (−6, −13, 19, 32 and 51 Btu/ft^2-h), respectively (Table 1).

Wind-velocity and temperature data were collected from a nearby weather station. Average velocity and average temperature over the selected two months of winter (December 2013 to January 2014) and summer (June 2014 to July 2014) were used as input conditions for simulation. Figure 3 shows the variations of temperature and wind speed around the mine from Dec. 1, 2013, to Jan. 31, 2014. Temperature and wind direction fluctuated over the selected periods. However, wind speed remained mostly within a range. For the simulation, the East boundary was modeled as the inlet boundary assuming an east-to-west airflow, due to the common occurrence of westbound flow most of the time. The input values for the summer and winter seasons are shown in Table 1. Variable temperature and variable heat flux inputs were avoided for simplification and due to the limitations of the software. However, wind velocity in an openpit mine is rarely constant over different elevations. In order to capture this variability in wind velocity, the East boundary was defined as the Velocity boundary with a power-law profile of velocity (Flores et al., 2013; Cheng, 2007).

Modeling domain

Two idealized geometries are used for simulation. The idealized pits have several advantages over the actual openpit domain: (1) idealized domains contain no faceted topography due to the simplified geometry; (2) mesh quality is excellent due to the absence of vertices and ridges; (3) good resolution in solution can be achieved with comparatively larger elements compared with an actual pit domain, due to planner pit surface; (4) there are fewer mesh elements; and (5) steady state is reached more quickly than an actual pit domain. The simulation of idealized pit domains, using boundary and initial conditions similar to those of an actual pit domain, provides quick results that can be used to evaluate various processes resulting in air recirculation inside the pit. Furthermore, the requirement for mesh resizing for a required resolution and an understanding of fugitive dust dispersion phenomenon inside the openpit mine can be realized.

The trapezoidal and conical openpit domains used for this study are presented in Figs. 4a and 4b, respectively. The pit cavities contain approximately the same volume as an actual openpit domain. The agreement in simulation results of both the trapezoidal and conical domains reflects the appropriate choice of simulation setup. Due to the geometry profiles of the domains, it is presumed that the dust dispersion phenomena in the conical domain will be of reduced duration compared with the trapezoidal domain. However, as the actual pit geometry is complex compared with the idealized geometries, higher fugitive dust retention is expected in the actual pit domain in comparison to the idealized domains. The ultimate pit slope is 40° for both the geometries. The numbers of mesh elements are in the order of 1.2 million and 1.3 million for the trapezoidal and conical domains, respectively. The mesh elements at the roughness boundary range from 6 to 12 m (20 to 40 ft), which resulted in the y+ distribution (Flores et al., 2014) between 30 and 10,000. y+ is the distance between the centroid of the first cell and the wall in wall units. The free atmosphere (FA) boundary is located 600 m (1,968 ft) from the surface. In high-latitude mines, the convective boundary layers may reach an elevation of between 300 and 600 m (984 and 1,968 ft) during winter (Hartmann and Wendler, 2005; Malingowski et al., 2014).

Simulation setup

Initial conditions, boundary conditions, choice of turbulence model and turbulent parameters were defined in the Analysis Condition wizard of the Cradle SC/Tetra preprocessor. Along with other setups, the generation and tracking of fugitive dust particles also needed to be defined, which could be done by the SC/Tetra's particle-tracking function.

Boundary conditions. All boundaries had to be defined to initiate a simulation. An inlet (East) and an outlet (West)

boundary (Figs. 4a and 4b) along with various wall boundaries were used for the simulation. Each inlet boundary was defined as the velocity boundary with a power-law profile of velocity (Fig. 5a) acting normally to the East boundary and at a constant inlet temperature, according to the season. The power-law equation of velocity profile is given by Eq. (3). A wind velocity of zero m/s (0 ft/sec) was assigned to the z-coordinate of 397.8 m (1,305 ft) since that z-coordinate was the lowest point on the East boundary. The outlet boundary was defined as the natural inflow/outflow boundary with inflow suppression (Bhowmick et al., 2015):

$$U = u * \left(\frac{dz_i}{dZ_{ref}}\right)^{\frac{1}{7}} \quad (3)$$

where U = velocity at height z, u = velocity at Z_{ref}, dz_i = distance between the ith and lowest points, and dZ_{ref} = distance between Z_{ref} and the lowest point.

The pit boundary, which is a surface of the mine, was defined as a rough wall with equivalent roughness of 0.02 m (0.066 ft) and a constant heat flux generated from the interface (Stull, 1988). The equivalent roughness generates mechanical turbulence in interaction with the wind speed. The constant heat flux generates the net radiation at the pit surface that results in sensible heat flux inside the air volume. This sensible heat flux warms or cools the air, resulting in the development of thermal buoyancy inside the openpit domain.

The North, South and FA boundaries were defined as free-slip wall boundaries with adiabatic heat transfer. The North, South and FA boundaries are required to enclose the volume of the domain. Free-slip wall conditions model these boundaries as a symmetry plane. In this study, a clear-sky condition was modeled, which assumes zero reflected LW radiation from the FA boundary. The adiabatic heat transfer conditions model these boundaries for a clear-sky condition.

Initial conditions. A steady-state condition was used as an initial velocity condition for the transient simulation. Inclusion of a steady-state condition defines the topography-induced downwind recirculation inside the pit (Bhowmick et al., 2015). To develop the thermal boundary layers and the flow regimes for various temperatures inside the pit, the simulation was run for two initial hours with a constant heat flux and temperature input. The simulation developed the turbulence due to thermal buoyancy while the mechanical turbulence in the domain was developed at the steady state. The fugitive dust particles were injected after two hours of initial simulation so that the transport of fugitive dust was carried out by the developed airflow. Figure 5b displays a velocity vector profile of the trapezoidal domain along the y = 896 m (2,940 ft) plane after two hours of simulation. The thermal buoyancy is observed to modify the purely mechanical-turbulence-induced flow pattern and an enlarged recirculation pattern is visible inside the openpit domain.

Turbulent flow and turbulence model. To model the thermal buoyancy, Boussinesq approximation was used in the Reynolds-averaged Navier-Stokes (RANS)-based standard kappa-epsilon turbulence model. This approximation accounts for change in density by the incompressible ideal gas law. This implies that density is a function of temperature alone and pressure is assumed to be constant. Therefore, buoyancy occurs when a temperature gradient develops between the air layers.

Fugitive dust sources and particle tracking. To study the fugitive dust dispersion phenomenon inside the selected openpit mine in different seasons, sources of dust were defined for several working locations in the mine. For both the idealized domains, a total of 25 dust source polygons were defined. The dust source polygons were positioned to represent various possible combinations of working locations and the simulation results can be processed to have estimations of fugitive dust retention from all possible fugitive dust sources. Each source was located approximately 10 m (33 ft) above the pit surface. This positioning of the dust sourc-

Figure 5

(a) Power-law velocity profile at East boundary (b) Velocity vector profile of the trapezoidal domain.

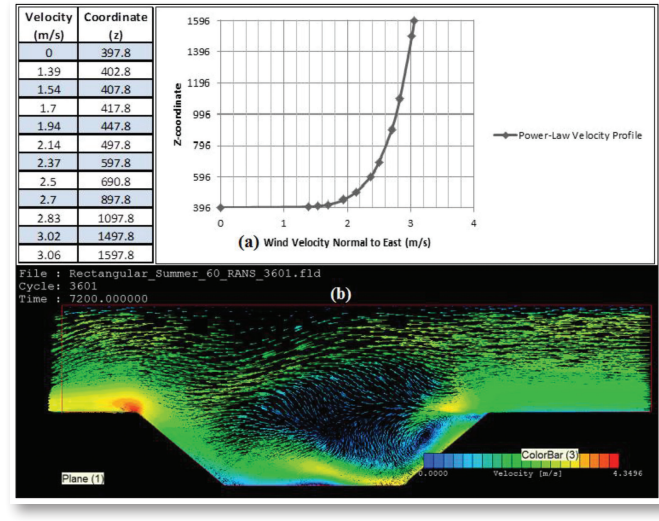

Figure 6

Dust sources in the trapezoidal domain.

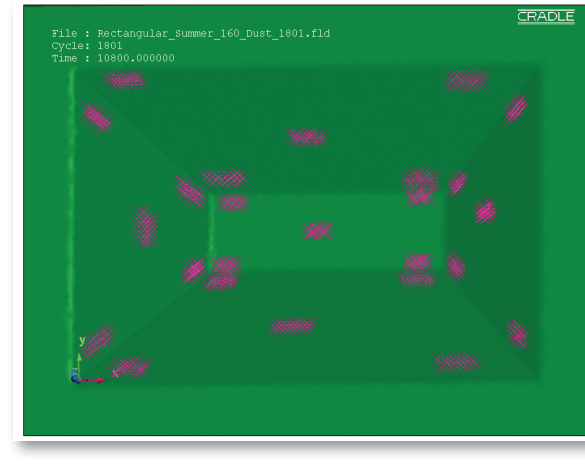

Figure 7

Velocity vector profile in the trapezoidal domain for (a) extreme insolation and (b) extreme winter. Temperature contour profile and locations of dust particles (black dots) in the trapezoidal domain for (c) extreme insolation and (d) extreme winter.

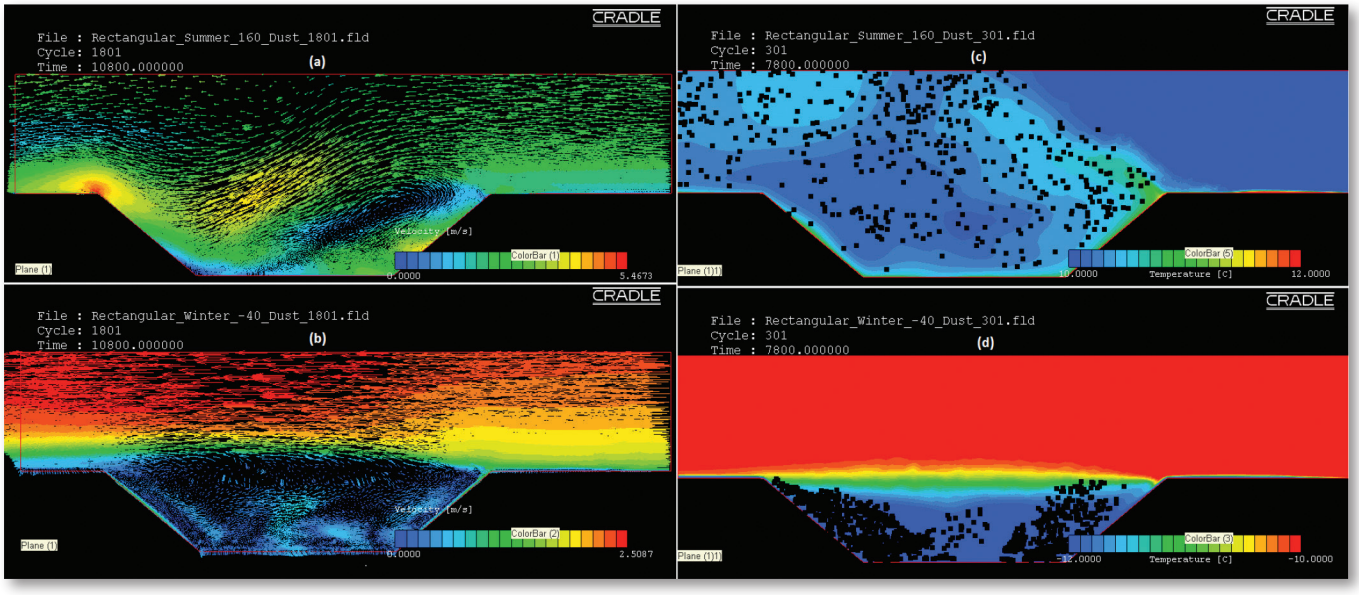

Figure 8

Pathlines of dust particles in the trapezoidal domain in (a) extreme insolation and (b) extreme winter conditions.

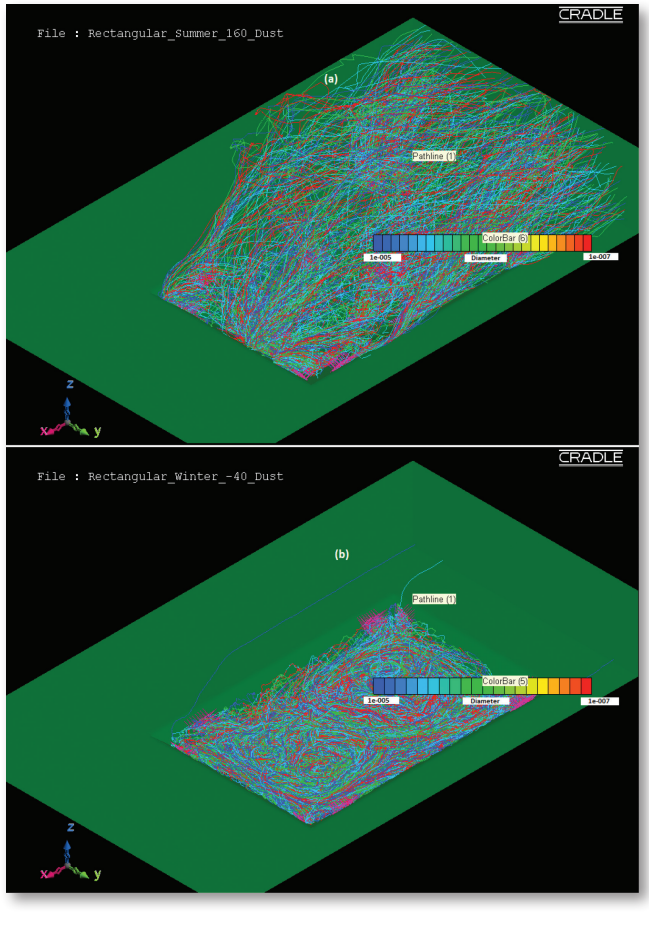

es takes into account two very important considerations: (1) Dust particles lying on the pit surface, where the airflow velocity is very close to zero, are not generally the source of fugitive dust, and these particles have very little probability to be dispersed by airflow; (2) The sources of fugitive dust, such as blasting, create dust volumes at various heights from the surface. The particles are thrown upward by the kinetic energy during blasting, and small-diameter particles (particulate matter, or PM) stay in suspension in the air and are eventually dispersed by the natural airflow. Figure 6 displays the 25 dust sources with the number of dust particles in the trapezoidal domain.

The particle-tracking function of Cradle SC/Tetra provides several options for defining the particles inside the CFD domain. The function can generate two types of particles (Software Cradle, 2013): (1) Marker particles: These particles have no mass and the velocity of a particle is the sum of flow velocity and sedimentation velocity. Since the sedimentation velocity of a marker particle is zero, these particles move with the flow. (2) Mass particles: These particles have mass, and they interact with the flow. Each source needs to be defined with the number of particles it generates. Due to the extensive requirement of computational space, the number of particles from each source was kept to 100 only. In this study, all particles were defined by the mass of the particle as dust particles have density and settling velocity. Four types of particles were generated from each source, as $PM_{0.1}$, $PM_{2.5}$, PM_5 and PM_{10}. The number of each type of particles from each source is 25, which is called the effective number (Software Cradle, 2013) and can be correlated based on field data. If the amount of retention of dust from a dust source location after two hours of simulation is 20 particles out of a total of 100 particles,

this simulation result estimates 20 percent retention of fugitive dust for that specific climatic condition, which can be cross-verified with the dust sampling data.

Results

The initial simulation of two hours was to develop the flow regimes. The particles were then injected and the simulation run until the last dust particle was removed. In order to analyze the dust dispersion phenomenon, a good understanding of the airflow regimes is important, since the retention of fugitive dust inside the domain is affected directly by the flow inside the mine cavity.

Airflow regimes in summer and winter. The airflow pattern inside the domain changes from summer to winter due to the amount of available heat flux. Even at the extreme insolation condition, different airflow patterns are exhibited when compared with a moderate insolation condition in summer. Figures 7a and 7b shows the airflow patterns along the y = 896 m (2,940 ft) plane inside the trapezoidal domain after three hours of simulation for an extreme insolation (160 W/m^2, or 51 Btu/ft^2-h, heat flux) condition and an extreme winter (-40 W/m^2, or -13 Btu/ft^2-h, heat flux) condition, respectively.

Tracking of particles. In Cradle SC/Tetra, the positions of the particles are updated during each time step. The locations of the particles during the simulation are reported at 10-minute intervals. Figures 7c and 7d display a temperature contour plot and the locations of dust particles (as black dots) 10 minutes after the particle injection for the extreme insolation and extreme winter conditions inside the trapezoidal domain, respectively.

As shown in Fig. 7c, the dust particles were dispersed all around the domain in the summer conditions. All of the dust particles were either transported out of the pit or settled down on the pit surface within one hour. The recirculation profile and the entrance of airflow in the pit cavity (Fig. 7a) also confirm the dust dispersion behavior (Fig. 7c). In the winter conditions (Fig. 7d), the temperature contours show the formation of atmospheric inversion (Collingwood et al., 2012) near the pit rim as the cold and dense air volume occupied the entire pit cavity (Fig. 7b). The air volume inside the pit cavity was completely detached from the airflow above the pit rim. As the wind speed inside the pit cavity was very close to zero, the dust particles generated inside the pit cavity were not transported outside the pit rim (Fig. 7d). Only a few particles reported outside the pit cavity in the extreme and moderate winter conditions in both domains, due to the atmospheric inversion near the pit rim. It resulted in high retention of dust particles inside the pit, and the particles were only removed when they settled down on the pit surface. The simulations for the winter conditions were run for a period of 26 hr from the injection of dust particles. Only 0.12 and 4.14 percent of the total particles were transported outside the pit domain for the extreme winter and moderate winter conditions, respectively.

Pathline of dust particles. The pathline of a particle can be generated based on its locations at different time steps. Figure 8 displays the pathlines of all of the dust particles of various diameters generated inside the pit domain for extreme insolation and extreme winter conditions. Figure 8b shows extensive fugitive dust retention in the extreme winter conditions due to the inversion. Only three pathlines of three dust particles out of a total of 2,500 generated dust particles are observed to report outside the inversion layer at the pit rim level and finally to be transported out of the domain. In the summer conditions (Fig. 8a), the dust-particle pathlines are observed to be distributed all around the model domain, with the direction of movement toward the outlet boundary.

Table 2

Summary of results for different climatic conditions.

Domain	Climate condition	Heat flux (W/m^2)	Percent settled down	Percent reported outside	Time to clear out
Trapezoidal	Moderate winter	−20	~92	4.14	>> 26 hr
	Extreme winter	−40	~96	0.12	>> 26 hr
	Fair insolation	60	73	27	52 min
	Moderate insolation	100	81	19	48 min
	Extreme insolation	160	75	25	53 min
Conical	Moderate winter	−20	~89	6.06	>> 26 hr
	Extreme winter	−40	~88	0.53	>> 26 hr
	Fair insolation	60	55	45	36 min
	Moderate insolation	100	61	39	32 min
	Extreme insolation	160	72	28	48 min

Summary of simulation results. The percentages of dust particles settled down on the pit surface and transported outside the pit domain and the time of dust retention inside each domain, collected for each of the climatic conditions, are presented in Table 2. The percentages were calculated based on the ratio of available dust particles to the actual number of generated dust particles. The simulation results of the trapezoidal and conical domains both show extensive fugitive dust retention for the winter conditions. Even after 26 hr of simulation, a considerable amount of dust particles neither settled down inside nor transported outside the domain and remained trapped below the inversion layer in both the domains. For the simulation of summer conditions, the airborne dust particles were transported outside the openpit domain within 45 to 55 minutes in the case of the trapezoidal domain and within 30 to 50 minutes in the case of the conical domain.

Conclusions

Four-component net-radiation sensors and temperature sensors installed inside an openpit mine and data from weather stations provided inputs for the modeling of dust dispersion. Based on the various climatic conditions, different input parameters were categorized for simulation. The winter season was simulated for moderate and extreme winter conditions based on the intensity of winter, while model domains for the summer season were simulated for fair, moderate and extreme summer conditions based on the intensity of insolation. Two idealized domains were simulated for the various choices of boundary conditions, and the amounts of fugitive dust retention from various dust sources were estimated. The simulation results displayed completely different dust-dispersion phenomena in summer and winter. Under winter conditions, the development of atmospheric inversion significantly affected the amount of dust retention inside the openpit domain. Under summer conditions, the airborne dust particles were transported outside the openpit domain within a short time. ■

Acknowledgments

The authors would like to acknowledge the National Institute for Occupational Safety and Health (NIOSH) for its financial support of this research. Technical support from Cradle North America's technical support team is also gratefully acknowledged.

References

Alvarez, J.T., Alvarez, I.D., Lougedo, S.T., and Hevia, B.G., 2007, "A CFD Lagrangian particle model to analyze the dust dispersion problem in quarries blast," *Computational Methods in Multiphase Flow IV, WIT Transactions on Engineering Sciences*, Vol. 56, WIT Press, ISSN 1743-3533 (online), pp. 9-18.

Bhowmick, T., Raj, K.V., and Bandopadhyay, S., 2015, "Constraints and Consequences in 3-Dimensional CFD Modeling of Openpit Mines," Preprint No.15-017, SME Annual Meeting, Denver, CO, Society for Mining, Metallurgy and Exploration Inc., Englewood, CO, pp. 1-6.

Cheng, N-S., 2007, "Power-law index for velocity profiles in open channel flows, advances in water resources," doi: 10.1016/j.advwatres.2007.02.001.

Collingwood, W., Raj, K.V., Choudhury, A., and Bandopadhyay, S., 2012, "CFD modeling of air flow in an openpit mine," *Mining Engineering*, Vol. 64, No. 2, pp. 44-50.

Flores, F., Garreaud, R., and Muñoz, R.C., 2014, "OpenFOAM applied to the CFD simulation of turbulent buoyant atmospheric flows and pollutant dispersion inside large open pit mines under intense insolation," *Computers & Fluids*, Vol. 90, pp. 72-87.

Flores, F., Garreaud, R., and Muñoz R.C., 2013, "CFD simulations of turbulent buoyant atmospheric flows over complex geometry: solver development in OpenFOAM," *Computers & Fluids*, Vol. 82, pp. 1-13.

Hartmann, B., and Wendler, G., 2005, "Climatology of the winter surface temperature inversion in Fairbanks, Alaska," *85th AMS Annual Meeting*, San Diego, CA, p. 187.

Malingowski, J., Atkinson, D., Fochesatto, J., Cherry, J., and Stevens, E., 2014, "An observational study of radiation temperature inversions in Fairbanks, Alaska," *Polar Science*, Vol. 8, pp. 24-39, doi: 10.1016/j.polar.2014.01.002.

Shi, Y., Feng, X., and Wei, F., 2000, "Three-dimensional non-hydrostatic numerical simulation for the PBL of an openpit mine," *Boundary-Layer Meteorology*, Vol. 94, Issue 2, pp. 197-224.

Software Cradle Co. Ltd., 2013, "User's Guide Preprocessor Reference," SC/Tetra Version 11.

Stull, R., 1988, *An Introduction to Boundary Layer Meteorology*, Kluwer Academic Publishers, p. 380.

Torno, S., Torano, J., Menendez, M., and Gent, M., 2011, "CFD simulation of blasting dust for the design of physical barriers", *Environmental Earth Sciences*, Vol. 64, doi 10.1007/s12665-010-0818-6, pp. 73-83.